JOURNAL OF THERMOPHYSICS AND HEAT TRANSFER
Vol. 20, No. 1, January–March 2006

Technical Notes

TECHNICAL NOTES are short manuscripts describing new developments or important results of a preliminary nature. These Notes should not exceed 2500 words (where a figure or table counts as 200 words). Following informal review by the Editors, they may be published within a few months of the date of receipt. Style requirements are the same as for regular contributions (see inside back cover).

Impingement Heat Transfer with a Nonlinear First-Order k–ε Model

Bart Merci,* Karim Van Maele,† and Erik Dick‡
Ghent University-UGent, B-9000 Ghent, Belgium

Nomenclature

D	=	nozzle diameter
D_h	=	hydraulic diameter
f_{R_y}	=	blending function
H	=	nozzle-plate distance
h	=	convection coefficient
k	=	turbulent kinetic energy
Nu	=	Nusselt number
$\bar{n}$	=	unit normal vector
P	=	impingement detector
Re	=	Reynolds number
R_y	=	dimensionless distance from solid boundary, $= \rho\sqrt{k}y/\mu$
S	=	strain rate, $= (2S_{ij}S_{ij})^{1/2}$
$\bar{\bar{S}}$	=	strain-rate tensor
W	=	nozzle width/impingement detector
y	=	normal distance from nearest solid boundary
ε	=	turbulent dissipation rate
η	=	dimensionless strain rate, $= \tau_t(S^2 + \Omega^2)^{1/2}$
κ	=	molecular thermal conductivity
μ	=	molecular viscosity
μ_t	=	turbulent or eddy viscosity
ρ	=	density
τ_t	=	turbulence timescale
Ω	=	vorticity, $= (2\Omega_{ij}\Omega_{ij})^{1/2}$

Introduction

In a previous paper,[1] it was shown that a first-order, but nonlinear eddy-viscosity turbulence model is sufficient to retain the heat-transfer accuracy of a cubic k–ε model[2] for axisymmetric turbulent jets, impinging onto a flat plate. A comparable level of accuracy was achieved as with Durbin's v^2–f model.[3–5]

However, the flow impingement detector, suppressing production of turbulent kinetic energy in stagnation flow regions,[1,2] was identically zero for two-dimensional flows, limiting the model's applicability to three-dimensional (or axisymmetric) flows. In the current Note, a more general impingement detector is introduced. It substantially improves heat-transfer predictions for the two-dimensional jet impinging onto a flat plate, while the accuracy is maintained for the round jet.

The turbulence model also contains a turbulent length-scale limiter in the transport equation for the dissipation rate.[1,2] It is investigated whether it is beneficial to replace it by an expression that does not contain the distance from the nearest solid boundary. This does not appear to be the case.

In general, accurate turbulent impingement heat-transfer results are obtained for various configurations (two-dimensional and axisymmetric flows with different nozzle-plate distances) and different Reynolds numbers.

Governing Equations

The governing equations are standard and reported elsewhere.[1] Only the differences between the turbulence model of the earlier work[1] and the current model are described here.

The impingement term I in $c_\mu = (4 + A_s\eta + I)^{-1}$ was defined as[1,2]

$$I_{\text{old}} = 25(1 - f_{R_y})|W| \tag{1}$$

with the blending function f_{R_y} going from 0 to 1 in the interval $R_y = \rho\sqrt{k}y/\mu = 1000$ to $R_y = 2000$. The quantity W is defined as[6] $W = 2^{1.5}S_{ij}S_{jk}S_{ki}/S^3$ and takes on the value $|W| = 1/\sqrt{6}$ in axisymmetric expansions or contractions (which occur in axisymmetric impingement regions) and becomes zero in shear flows. However, a major disadvantage is that $|W|$ is identically zero for all two-dimensional flows. As a consequence, the impingement term remains zero for a two-dimensional jet, impinging onto a plate. As will be illustrated, results severely deteriorate for two-dimensional impingement heat transfer.

Therefore, the impingement term of Manceau[7] is used, with parameter P:

$$P = \frac{|\text{trace}(\bar{\bar{S}}\bar{\bar{M}})|}{\sqrt{2}S} \tag{2}$$

with the tensor $\bar{\bar{M}}$:

$$M_{ij} = n_i n_j - \tfrac{1}{3}\delta_{ij} \tag{3}$$

where n_i is the i component of the unity vector, normal to the nearest solid boundary. $P = 1/\sqrt{6}$ in axisymmetric impingement flow regions (which is the same value as $|W|$ as just described), and $P = 1/\sqrt{8}$ in two-dimensional impingement flow regions (as opposed to zero for $|W|$). The parameter is zero for shear flows.

The impingement term I, based on P, is defined as

$$I_{\text{Man}} = 40(1 - f_{R_y})P \tag{4}$$

In the discussion of the results, it is illustrated that the impingement detector, based on P, is indeed active in both axisymmetric and two-dimensional impingement flows, but that it is active in a more narrow region than the detector, based on $|W|$. As a consequence, the factor 40 could be chosen in order to obtain more accurate stagnation heat-transfer rates. With Eq. (1), this was not possible because

Received 23 December 2004; revision received 3 March 2005; accepted for publication 3 March 2005.

*Postdoctoral Fellow of the Fund of Scientific Research, Flanders (Belgium) (FWO-Vlaanderen); and Professor, Department of Flow, Heat and Combustion Mechanics, Sint-Pietersnieuwstraat 41; Bart.Merci@UGent.be. Member AIAA.

†Researcher, Department of Flow, Heat and Combustion Mechanics, Sint-Pietersnieuwstraat 41.

‡Professor, Department of Flow, Heat and Combustion Mechanics, Sint-Pietersnieuwstraat 41. Member AIAA.

increasing the factor 25 up to 40 improved stagnation heat-transfer rate predictions, but at the cost of underpredicted heat transfer outside of the stagnation region. On the other hand, the local character of Eq. (4) has the disadvantage that the heat-transfer rate is somewhat overpredicted outside of the stagnation region. Therefore, the following expression for I is applied:

$$I_{\text{present}} = \max(I_{\text{old}};\, I_{\text{Man}}) \tag{5}$$

This is further illustrated in the Results section.

In the dissipation-rate transport equation, the following turbulent length-scale limiter was introduced[1]:

$$L = 0.83(\varepsilon^2/k)\max\left[(l_t/l_e - 1)(l_t/l_e)^2;\, 0\right] \tag{6}$$

with

$$l_t = k^{\frac{3}{2}}/\varepsilon \tag{7}$$

Indeed, when l_t becomes larger than a certain equilibrium length scale l_e, the additional source term increases the dissipation rate, and as such lower values of turbulent kinetic energy are obtained. Consequently, the length scale l_t becomes smaller. There is, however, some freedom in the definition of l_e. It was defined as[1,2]

$$l_{e,\,\text{orig}} = 2.55y \tag{8}$$

Pope[8] shows that this is valid for the logarithmic layer in a fully developed channel flow. In the $v^2 - f$ model,[4,5] on the other hand, a limitation on the turbulent length scale is based on an (equilibrium) length scale proportional to $\sqrt{k}/S$. Here, this is generalized to a length scale proportional to $\sqrt{k}/(S^2+\Omega^2)^{1/2}$. Noting that in the log layer in a channel flow[8] $(S^2+\Omega^2)^{\frac{1}{2}}k/\varepsilon = 3\sqrt{2}$ and expressing that $l_t = l_e$ in that region leads to the alternative definition:

$$l_{e,\,\text{alt}} = 3\sqrt{2}\left(\sqrt{k}\tau_t\right/\eta) \tag{9}$$

In the Results section, it is illustrated that this is a valid alternative, but is active only in a more narrow region than the classical expression (8). In the final model formulation (present), Eq. (8) is used.

Test Cases

As previously,[1] the equations are solved with the commercial computational-fluid-dynamics package FLUENT, with second-order upwinding for the convective terms in the momentum, energy, and turbulence equations. The SIMPLE algorithm is used for the pressure-velocity coupling. All results have been checked with respect to grid independence.[1]

In the axisymmetric test case, the turbulent jet emerges as a fully developed flow from a round nozzle exit. The Reynolds number, based on mean velocity and nozzle diameter, is $Re = 2.3 \times 10^4$ or $Re = 7 \times 10^4$. The nozzle-plate distances, considered here, are $H = 2D$ and $H = 6D$. The pipe thickness is $0.0313D$, and a coflow airstream is established through entrainment. A uniform small heat flux is imposed at the plate onto which the jet impinges. Local heat-transfer measurements have been performed by several groups.[9–12] The simulations have been performed on a structured mesh (256×224 cells) that starts $D/2$ upstream of the nozzle exit in order to correctly reproduce the air entrainment. The nozzle exit is positioned at $x = 0$. The cells are stretched in the axial direction toward $x = H/2$ and then again refined toward the plat ($x = H$). Radially, there are 80 cells within the pipe. For accuracy reasons near the stagnation point, the mesh is refined toward the symmetry axis. Toward the nozzle edge, the cells are also refined for the air entrainment prediction. The cells are stretched toward the outer radial boundary (positioned at $r = 10D$).

In the two-dimensional test case[13] the jet-exit Reynolds number, based on mean velocity and hydraulic diameter D_h (i.e., equal to twice the jet width W), is $Re = 2.25 \times 10^4$. The nozzle-plate distance, considered here, is $H = 3.5D_h = 7W$. The turbulence intensity is reported to be 3.5% at the nozzle exit. The jet width equals 0.0127 m (while its transversal length is 0.26 m). The solid nozzle width is 0.061 m (including the 0.0127-m-wide jet). The plate, onto which the jet impinges, is heated in such a way that its temperature does not exceed ambient temperature by more than 15°C.

Numerically, the same policy has been used for the mesh as for the round jet test cases, replacing D by D_h. The only difference is that the grid does not extend upstream of the nozzle exit. The jet emerges from a thick nozzle (as just described), so that air entrainment is still accurately described, even when the computational domain does not extend ahead of the nozzle exit.

For all cases, the local Nusselt number is defined as

$$Nu = hD_h/\kappa \tag{10}$$

The boundary conditions are as follows. At the jet inlet, mean velocity, temperature, and turbulent kinetic energy and dissipation rate are imposed. For the round jet, the inlet data are calculated from the assumption of fully developed flow, as this flow state was reported in the experiments. For the two-dimensional jet a uniform velocity inlet is imposed. As reported for that experiment, a turbulence intensity of 3.5% is applied.[13] The dissipation rate ε is computed as[14]

$$\varepsilon = c_\mu^{\frac{3}{4}} k^{\frac{3}{2}} \Big/ l_m \tag{11}$$

with $l_m = D_h/15$. Variations between an intensity of 1 to 10% yield variations of less than 3% in the stagnation-point Nusselt number, provided that ε is adjusted accordingly through Eq. (11). Pressure is extrapolated from the flowfield at the jet inlet. The coflow air entrainment is described by imposing atmospheric static pressure and temperature, while setting zero derivatives for all other quantities (pressure inlet). At the outer radial boundary, static pressure is imposed, as well as zero derivatives for all other quantities (pressure outlet). The plate onto which the jet impinges is uniformly heated (heat flux 50 W/m^2). Velocity components and turbulent kinetic energy are set to zero. The derivative of pressure is set to zero. The turbulent dissipation rate at the plate is[1,2]

$$\varepsilon_w = 2\left(\frac{\mu}{\rho}\right)\left(\frac{\partial\sqrt{k}}{\partial n}\right)^2$$

Results

Impingement Detector

Figure 1 presents local Nusselt-number profiles for the two-dimensional jet (Fig. 1a) and the round jet (Fig. 1b), impinging onto a flat plate. Three curves are compared to the experimental data: Merci[1], in which Eq. (1) is used as impingement expression; I_{Man}, with Eq. (4) as impingement term; and present, which refers to the complete present model, that is, with Eqs. (5) and (8).

The profiles for the plane jet reveal that the original impingement detector (1) does not work, as just explained. Consequently, the local heat transfer is severely overpredicted in the symmetry plane ($y = 0$). Away from the stagnation region (approximately $y > 0.5D_h$), the result is in good agreement with experimental data. For the present impingement detector (5), which reduces here to Eq. (4), the global profile is in very good agreement with the experimental data (curves I_{Man} and present coincide). Only in the region $0.5D_h < y < 1.5D_h$, a small underprediction is observed. This is mainly because of convection of lower values of turbulent kinetic energy from the symmetry axis into this region, as well as because of the reduced value of the eddy viscosity (reducing production of turbulent kinetic energy). This explains the lower Nusselt-number value.

The right-hand side of Fig. 1 illustrates the quality with the present model for the round jet. The very good agreement on the axis is not surprising, because the factor 40 in Eq. (4) was tuned on this test case. The difference between the curves Merci[1] and I_{Man} is caused by the impingement detector: in the former, expression (1) is applied, whereas in the latter Eq. (4) is used. Because on the stagnation line, $|W|$ and P take on the same value $(1/\sqrt{6})$, it is not surprising that the stagnation value is lower with Eq. (4) because of the impingement term in c_μ. Indeed, the value of c_μ (and thus $c_{\mu,\text{eff}}$) is lower, so that the eddy viscosity is lower, resulting in lower production of

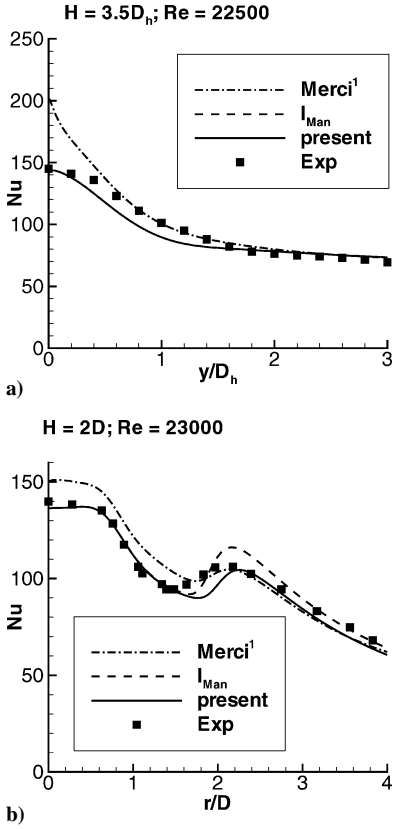

Fig. 1 Local Nusselt-number profiles for a) two-dimensional and b) axisymmetric jet impinging onto a flat plate.

turbulent kinetic energy and consequently lower local heat-transfer rate. On the other hand, the height of the secondary peak around $r = 2D$ for the I_{Man} curve reveals that impingement detector (4) is active in a more narrow region than Eq. (1) Indeed, the peak is higher than for the Merci[1] curve because of a higher value of c_μ. This also explains why previously[1,2] the factor 25 was chosen (instead of 40): it was a tradeoff between better stagnation-point predictions and a global downward shift of the Nusselt-number profile, resulting in less accurate agreement away from the stagnation region.

The present curve combines the advantages because the maximum is taken in Eq. (5). The slight under-prediction in the region $1.5r < D < 2.5r$ is caused by the same reasons as just explained for the two-dimensional jet.

Turbulent Length-Scale Limiter

The influence of the turbulent length-scale limiter L [Eq. (6)] and the differences between the choices of Eqs. (8) or (9) are illustrated in Fig. 2.

For the two-dimensional jet (left-hand side), it is observed that the introduction of L, with l_e from either Eqs. (8) or (9), does not affect the local Nusselt-number profile at all, when the impingement term (5) is used in c_μ: curves I_{Man}; $L = 0$ (no length-scale limiter), I_{Man}; $l_{e,\text{alt}}$ [using Eq. (9)] and present [using Eq. (8)], coincide. The turbulent length-scale limiter L does not interfere with the results because the length scale is already sufficiently small as a result of the reduction of c_μ (and thus the turbulent kinetic energy) through the impingement term.

The effect of L [with Eq. (8)] is visible when $I = 0$, as was the case with the previous impingement detector. Indeed, there is a reduction in the stagnation-point heat transfer (curve Merci[1] compared to Merci,[1] $L = 0$) when L is introduced into the ε transport equation. However, this is not sufficient to obtain a reasonable level of accuracy. In general, the influence of L is much smaller than the influence of the impingement term.

For the axisymmetric case (right-hand side), these observations are confirmed. A drastic overprediction of stagnation heat transfer

Table 1 Stagnation-point Nusselt number for round jets

Model	$v^2 - f^4$	Merci[1]	Present	Exp.
$Re = 2.3 \times 10^4$, $H = 6D$	178	156	145	145–185
$Re = 7 \times 10^4$, $H = 2D$	265	264	247	$235 \pm 5\%$
$Re = 7 \times 10^4$, $H = 6D$	300	290	261	$275 \pm 5\%$

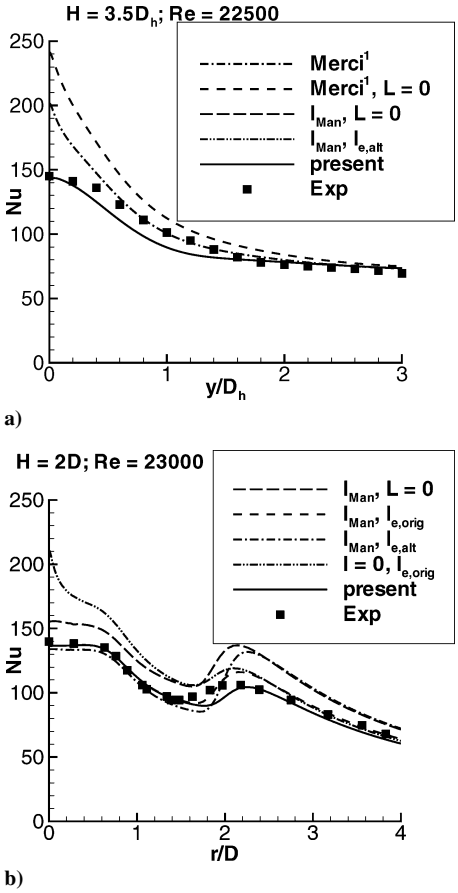

Fig. 2 Influence of length-scale limiter on local Nusselt-number profiles for a) two-dimensional and b) axisymmetric jet impinging onto a flat plate.

is revealed when the impingement term is set to zero, whereas the length-scale limiter L is applied [with Eq. (8)], as illustrated by curve $I = 0$; $l_{e,\text{orig}}$. On the other hand, when L is set to zero, whereas Eq. (4) is used as impingement term (curve I_{Man}; $L = 0$), the overprediction is much less severe. This confirms that the length-scale limiter plays a minor role, compared to the impingement term.

The influence of the choice l_e from Eqs. (8) or (9) is illustrated by the difference between curves I_{Man}; $L = 0$, I_{Man}; $l_{e,\text{orig}}$, and I_{Man}; $l_{e,\text{alt}}$. A global downward shift is observed from the profile for $L = 0$, when Eq. (8) is applied (note that for $r < 2D$, curve I_{Man}; $l_{e,\text{orig}}$ coincides with curve present). When Eq. (9) is used, differences are small as long as $r < 2D$, but then a much higher secondary peak is observed: the turbulent length scale is no longer active for $r > 2D$, and the curve practically coincides with the curve for $L = 0$. This shows that the length-scale limiter L is active in a more narrow region than when Eq. (8) is used. Because this deteriorates the results, expression (8) has been kept in the present model. This has the advantage that the local character of the impingement term is complementary with the global character of the length-scale limiter, so that accurate results can be obtained both inside and outside the stagnation region.

Other Configurations

Table 1 shows the stagnation-point heat transfer for the round jet for different nozzle-plate distances and different Reynolds numbers.

The quality remains comparable to the v^2-f model results and our previous model formulation. Note that the distance $H = 6D$ corresponds to heat transfer behind the jet potential core (as opposed to $H = 2D$).

Conclusions

Accurate numerical impingement heat-transfer results have been obtained with the presented nonlinear, but first-order, $k-\varepsilon$ model. Results were presented for both two-dimensional and axisymmetric impingement heat transfer at different Reynolds numbers and for different geometrical configurations. The improvement over previous work is caused by a novel impingement detector, which is now also active in two-dimensional flows so that a substantial increase in accuracy is obtained for such cases. For the axisymmetric test cases, the quality has also been slightly improved.

It has been illustrated that the introduction of a turbulent length-scale limiter in the transport equation for the turbulent dissipation rate has some beneficial effect when the turbulent kinetic energy is still overpredicted after the impingement term has been introduced. However, the effect of the length-scale limiter is much smaller than that of the impingement term. An alternative choice for the equilibrium length scale, used as the limiting value, based on the strain rate, does not improve the results. Therefore, the original formulation with respect hereto, based on the distance from the nearest solid boundary, has been retained.

References

[1]Merci, B., De Langhe, C., Lodefier, K., and Dick, E., "Axisymmetric Impingement Heat Transfer with a Non-Linear $k-\varepsilon$ Model," *Journal of Thermophysics and Heat Transfer*, Vol. 18, No. 1, 2004, pp. 100–107.

[2]Merci, B., and Dick, E., "Heat Transfer Predictions with a Cubic $k-\varepsilon$ Model for Axisymmetric Turbulent Jets Impinging onto a Flat Plate," *International Journal of Heat and Mass Transfer*, Vol. 46, No. 3, 2003, pp. 469–480.

[3]Durbin, P., "Near-Wall Turbulence Closure Without Damping Functions," *Theoretical and Computational Fluid Dynamics*, Vol. 3, No. 1, 1991, pp. 1–13.

[4]Behnia, M., Parneix, S., and Durbin, P. A., "Prediction of Heat Transfer in an Axisymmetric Turbulent Jet Impinging on a Flat Plate," *International Journal of Heat and Mass Transfer*, Vol. 41, No. 12, 1998, pp. 1845–1855.

[5]Behnia, M., Parneix, S., Shabany, Y., and Durbin, P. A., "Numerical Study of Turbulent Heat Transfer in Confined and Unconfined Impinging Jets," *International Journal of Heat and Fluid Flow*, Vol. 20, No. 1, 1999, pp. 1–9.

[6]Shih, T. H., Liou, W. W., Shabbir, A., Yang, Z., and Zhu, J., "A New $k-\varepsilon$ Eddy Viscosity Model for High Reynolds Number Turbulent Flows," *Computers and Fluids*, Vol. 24, No. 3, 1995, pp. 227–238.

[7]Manceau, R., "Accounting for Wall-Induced Reynolds Stress Anisotropy in Explicit Algebraic Stress Models," *Proceedings of the Third International Symposium on Turbulence and Shear Flow Phenomena*, edited by N. Kasagi, J. K. Eaton, R. Friedrich, J. A. C. Humphrey, M. A. Leschziner, and T. Miyauchi, Vol. I, Sendai, Japan, 2003, pp. 39–44.

[8]Pope, S. B., *Turbulent Flows*, 2nd ed., Cambridge Univ. Press, Cambridge, England, U.K., 2000, p. 288.

[9]Baughn, J. W., and Shimizu, S., "Heat Transfer Measurements from a Surface with Uniform Heat Flux and an Impinging Jet," *Journal of Heat Transfer*, Vol. 111, No. 4, 1989, pp. 1096–1098.

[10]Baughn, J. W., Hechanova, A., and Yan, X., "An Experimental Study of Entrainment Effects on the Heat Transfer from a Flat Surface to a Heated Circular Impinging Jet," *Journal of Heat Transfer*, Vol. 113, No. 4, 1991, pp. 1023–1025.

[11]Yan, X., "A Preheated-Wall Transient Method Using Liquid Crystals for the Measurement of Heat Transfer on External Surfaces and in Ducts," Ph.D. Dissertation, Univ. of California, Davis, 1993.

[12]Lytle, D., and Webb, B., "Air Jet Impingement Heat Transfer at Low Nozzle-Plate Spaces," *International Journal of Heat and Mass Transfer*, Vol. 37, No. 12, 1994, pp. 1687–1697.

[13]Narayanan, V., Seyed-Yagoobi, J., and Page, R. H., "An Experimental Study of Fluid Mechanics and Heat Transfer in an Impinging Slot Jet Flow," *International Journal of Heat and Mass Transfer*, Vol. 47, No. 12, 2004, pp. 1827–1845.

[14]Merci, B., Dick, E., Vierendeels, J., and De Langhe, C., "Determination of ε at Inlet Boundaries," *International Journal of Numerical Methods for Heat and Fluid Flow*, Vol. 12, No. 1, 2002, pp. 65–80.